# Synthesis and Biological Evaluation of Enantiomerically Pure (*R*)- and (*S*)-[$^{18}$F]OF-NB1 for Imaging the GluN2B Subunit-Containing NMDA receptors

**Marvin Korff**
Department of Radiology and Imaging Sciences, Emory University, 1364 Clifton Road, Atlanta, GA 30322, USA.
**Ahmad Chaudhary**
Department of Radiology and Imaging Sciences, Emory University, 1364 Clifton Road, Atlanta, GA 30322, USA.
**Yinlong Li**
Department of Radiology and Imaging Sciences, Emory University, 1364 Clifton Road, Atlanta, GA 30322, USA.
**Xin Zhou**
Department of Radiology and Imaging Sciences, Emory University, 1364 Clifton Road, Atlanta, GA 30322, USA.
**Chunyu Zhao**
Department of Radiology and Imaging Sciences, Emory University, 1364 Clifton Road, Atlanta, GA 30322, USA.
**Jian Rong**
Department of Radiology and Imaging Sciences, Emory University, 1364 Clifton Road, Atlanta, GA 30322, USA.
**Jiahui Chen**
Department of Radiology and Imaging Sciences, Emory University, 1364 Clifton Road, Atlanta, GA 30322, USA.
**Zhiwei Xiao**
Department of Radiology and Imaging Sciences, Emory University, 1364 Clifton Road, Atlanta, GA 30322, USA.
**Nehal H. Elghazawy**
Institute of Pharmacy, Department of Medicinal Chemistry, Martin-Luther-University Halle-Wittenberg, W.-Langenbeck-Str. 4, 06120 Halle, Germany.
**Wolfgang Sippl**
Institute of Pharmacy, Department of Medicinal Chemistry, Martin-Luther-University Halle-Wittenberg, W.-Langenbeck-Str. 4, 06120 Halle, Germany.

**April T. Davenport**
Department of Physiology and Pharmacology, Wake Forest School of Medicine, Winston Salem, NC 27157, USA.
**James B. Daunais**
Department of Physiology and Pharmacology, Wake Forest School of Medicine, Winston Salem, NC 27157, USA.
**Lu Wang**
Center of Cyclotron and PET Radiopharmaceuticals, Department of Nuclear Medicine and PET/CT-MRI Center, the First Affiliated Hospital of Jinan University, Guangzhou 510630, China.
**Carmen Abate**
Dipartimento di Farmacia-Scienze Del Farmaco, Università Degli Studi di Bari ALDO MORO, Via Orabona 4, Bari 70125, Italy.
**Hazem Ahmed**
Center for Radiopharmaceutical Sciences ETH-PSI-USZ, Institute of Pharmaceutical Sciences ETH, Vladimir-Prelog-Weg 4, 8093 Zurich, Switzerland.
**Ron Crowe**
Department of Radiology and Imaging Sciences, Emory University, 1364 Clifton Road, Atlanta, GA 30322, USA.
**Steven H. Liang**
Department of Radiology and Imaging Sciences, Emory University, 1364 Clifton Road, Atlanta, GA 30322, USA.
**Simon M. Ametamey**
Center for Radiopharmaceutical Sciences ETH-PSI-USZ, Institute of Pharmaceutical Sciences ETH, Vladimir-Prelog-Weg 4, 8093 Zurich, Switzerland.
**Bernhard Wünsch**
Institut für Pharmazeutische und Medizinische Chemie, Westfälische Wilhelms-Universität Münster, Corrensstraße 48, D-48149 Münster, Germany.
**Ahmed Haider** ( ahmed.haider@usz.ch )
Department of Radiology, Division of Nuclear Medicine and Molecular Imaging Massachusetts General Hospital and Harvard Medical School, 55 Fruit Street, Boston, MA 02114, USA https://orcid.org/0000-0002-5204-4473

---

**Research Article**

**Keywords:** N-methyl-D-aspartate (NMDA) receptor, probe development, translational molecular imaging, GluN2B antagonists, positron emission tomography (PET)

**Posted Date:** January 27th, 2023

**DOI:** https://doi.org/10.21203/rs.3.rs-2516002/v1

# Abstract

GluN2B subunit-containing *N*-methyl-d-aspartate (NMDA) receptors have been implicated in various neurological disorders. Nonetheless, a validated fluorine-18 labeled positron emission tomography (PET) ligand for GluN2B imaging in the living human brain is currently lacking. As part of our PET ligand development program, we have recently reported on the preclinical evaluation of [$^{18}$F]OF-NB1 – a GluN2B PET ligand with promising attributes for potential clinical translation. However, the further development of [$^{18}$F]OF-NB1 is currently precluded by major limitations in the radiolabeling procedure. These limitations include the use of highly corrosive reactants and racemization during the radiosynthesis. As such, the aim of this study was to develop a synthetic approach that allows an enantiomerically pure radiosynthesis of (*R*)-[$^{18}$F]OF-NB1 and (*S*)-[$^{18}$F]OF-NB1, as well as to assess their *in vitro* and *in vivo* performance characteristics for imaging the GluN2B subunit-containing NMDA receptor in rodents. A two-step radiosynthesis involving radiofluorination of the boronic acid pinacol ester, followed by coupling to the 3-benzazepine core structure via reductive amination was employed. The new synthetic approach yielded enantiomerically pure (*R*)-[$^{18}$F]OF-NB1 and (*S*)-[$^{18}$F]OF-NB1, while concurrently circumventing the use of corrosive reactants. *In vitro* autoradiograms with mouse and rat brain sections revealed a higher selectivity of (*R*)-[$^{18}$F]OF-NB1 over (*S*)-[$^{18}$F]OF-NB1 for GluN2B-rich brain regions. In concert with these observations, blockade studies with commercially available GluN2B antagonist, CP101606, showed a significant signal reduction, which was more pronounced for (*R*)-[$^{18}$F]OF-NB1 than for (*S*)-[$^{18}$F]OF-NB1. Conversely, blockade experiments with sigma2 ligand, FA10, did not result in a significant reduction of tracer binding for both enantiomers. PET imaging experiments with CD1 mice revealed a higher brain uptake and retention for (*R*)-[$^{18}$F]OF-NB1, as assessed by visual inspection and volumes of distribution from Logan graphical analyses. *In vivo* blocking experiments with sigma2 ligand, FA10, did not result in a significant reduction of the brain signal for both enantiomers, thus corroborating the selectivity over sigma2 receptors. In conclusion, we have developed a novel synthetic approach that is suitable for upscale to human use and allows the enantiomerically pure radiosynthesis of (*R*)-[$^{18}$F]OF-NB1 and (*S*)-[$^{18}$F]OF-NB1. While both enantiomers were selective over sigma2 receptors *in vitro* and *in vivo*, (*R*)-[$^{18}$F]OF-NB1 showed superior GluN2B subunit specificity by *in vitro* autoradiography and higher volumes of distribution in small animal PET studies.


# Introduction

*N*-methyl-d-aspartate (NMDA) receptors are ligand-gated ion channels that belong to the family of ionotropic glutamate receptors (iGluRs). Endowed with a remarkable variety of biological functions, NMDA receptors constitute heterotetrameric complexes composed of combinations of the subunits GluN1, which is processed in eight distinct splice variants, GluN2A-D, and GluN3A-B. [1–4] Typically, a functional NMDA receptor comprises two glycine-binding GluN1 subunits and at least one glutamate-binding GluN2 subunit. Simultaneous binding of glycine and glutamate initiates NMDA receptor activation, which involves voltage-dependent relief of magnesium blockade, depolarization of the postsynaptic membrane and calcium ion influx. [5–7] While NMDA receptors are key players in

neurophysiology, contributing to memory and learning via modulation of synaptic plasticity, the GluN2B subunit-carrying NMDA receptor has been implicated in the pathophysiology of various neurological disorders. [8–16] Indeed, the role of overstimulation of the excitatory GluN2B subunit in the development of several CNS-related pathologies has been corroborated, [17,18] whereas targeting GluN2B-mediated excitotoxicity has been suggested as a promising therapeutic strategy for various diseases, including Alzheimer's disease (AD), Parkinson's disease (PD), ischemic stroke, traumatic brain injury, neuropathic pain and depression. [19–30] Early efforts to develop NMDA receptor antagonists prompted the discovery of NMDA receptor channel blockers such as phencyclidine (PCP), thienylcyclohexylpiperidine (TCP), ketamine, memantine, and MK-801 (dizocilpine). Despite their well-documented therapeutic efficacy, most of these “broad-spectrum” antagonists were associated with a poor safety profile, potentially owing to the lack of subunit-selectivity. [17,31,32] As such, more recent attempts have focused on the development of GluN2B-selective antagonists, which has become feasible since the discovery of the *N*-terminal domain (NTD) binding site that is located at the interface between GluN1 and GluN2B. [33] Several GluN2B-selective antagonists have been reported to date – some of which have been advanced to humans, including CP101,606 (traxoprodil) [30], MK-0657 (CERC-301) [34] and EVT-101 (NCT01128452). Nonetheless, the development of a suitable GluN2B-selective antagonist for clinical use has proven challenging, at least in part, due to the lack of appropriate non-invasive imaging tools that allow the assessment of target engagement in the human brain.

Positron emission tomography (PET) constitutes a powerful non-invasive molecular imaging modality that allows real-time quantification of biochemical processes. [35] Accordingly, PET has been established as a reliable tool for CNS-targeted receptor quantification as well as target occupancy studies in preclinical and clinical research. [36] Given the translational relevance of visualizing drug-receptor interactions to facilitate the development of GluN2B antagonists in the pipeline, strenuous efforts have been devoted to the discovery of a suitable GluN2B PET radioligand in the past two decades. While numerous probes exhibited high *in vitro* specificity and selectivity towards the GluN2B subunit, the vast majority of reported ligands were plagued by unfavourable *in vivo* performance characteristics. [37] Major drawbacks included low brain penetration, lack of *in vivo* specificity and selectivity, as well as the presence of radiometabolites in the CNS. [37,38] We have recently reported on the first successful GluN2B subunit-selective PET radioligand, (*R*)-[$^{11}$C]Me-NB1, that proved to be suitable for visualizing GluN2B *in vitro* and *in vivo*. [39] The structure of (*R*)-[$^{11}$C]Me-NB1 belongs to a class of 3-benzazepine based ligands, encompassing a series of high-affinity GluN2B antagonists, that were first reported by Tewes et al. [40] Of note, (*R*)-[$^{11}$C]Me-NB1 was successfully translated to humans, rendering it the first and only GluN2B-targeted PET radioligand to be clinically validated to date. [41] Despite the outstanding performance characteristics, the use of (*R*)-[$^{11}$C]Me-NB1 is limited by the short physical half-life of carbon-11 (20.3 min), which confines the use of (*R*)-[$^{11}$C]Me-NB1 to facilities with an on-site cyclotron. As part of our efforts to develop a suitable radiofluorinated analog (physical half-life of fluorine-18, 109.8 min), that would allow satellite distribution to hospitals without an on-site cyclotron, we have synthesized and evaluated a series of fluorinated (*R*)-[$^{11}$C]Me-NB1 derivatives [42–49] – of which [$^{18}$F]OF-NB1 proved to be

particularly promising for translation into humans. However, the clinical translation of [$^{18}$F]OF-NB1 requires further optimization of the radiolabeling strategy. In particular, current radiolabeling routes utilize corrosive reactants such as boron tribromide and lead to racemization of enantiomerically pure precursors. However, based on previous observations with this class of compounds [41], it is anticipated that (*R*)- and (*S*)-[$^{18}$F]OF-NB1 may exhibit distinct enantiomeric behaviors with respect to GluN2B binding specificity and selectivity over sigma receptors. Along this line of reasoning, a synthetic approach that allows the enantiomerically pure synthesis of (*R*)-[$^{18}$F]OF-NB1 and (*S*)-[$^{18}$F]OF-NB1 without racemization is warranted to enable the evaluation of the enantiomers in future human studies. Thus, the aim of this study was to develop a synthesis strategy that is devoid of corrosive reactants and provides enantiomerically pure (*R*)-[$^{18}$F]OF-NB1 and (*S*)-[$^{18}$F]OF-NB1 suitable for human use, as well as to assess their *in vitro* and *in vivo* performance characteristics for imaging the GluN2B subunits of the NMDA receptor in rodents.

# Results And Discussion

While [$^{18}$F]OF-NB1 exhibited outstanding performance characteristics as a GluN2B subunit-targeted PET radioligand in preclinical experiments, the original radiosynthesis was plagued by the harsh conditions required to cleave the hydroxyl protecting groups, hampering automatization and clinical translation of the probe (Scheme 1, previous work). [50] Moreover, when employing enantiomerically pure precursor **1**, racemization of the center of chirality in benzyl position was observed during the reaction with boron tribromide, precluding the synthesis of enantiomerically pure (*R*)- or (*S*)-[$^{18}$F]OF-NB1. [49] We have now developed a novel synthesis strategy (Scheme 1, this work) that proceeds via a building block approach, thereby opening up several possibilities: (1) precursor **3** for the radiosynthesis does not contain any OH-groups, which alleviated the necessity of protection groups for the radiofluorination. (2) Starting from enantiomerically pure 3-benzazepine building block **5** allowed us to conduct radiolabeling of enantiomerically pure of (*R*)-[$^{18}$F]OF-NB1 and (*S*)-[$^{18}$F]OF-NB1. (3) Additionally, the novel strategy was faster and more effective compared to the linear two-step synthesis, since a chiral HPLC to separate the enantiomers at the end of the radiosynthesis was no longer required. (4) Finally, given the rapid nature of reductive aminations, our proposed building block approach is adoptable to a wide scope of substrates, including those containing functional groups that are not tolerated under nucleophilic radiofluorination conditions.

The concept of building block-based radiochemistry is well established in fluorine-18 chemistry for a variety of reactions [51, 52], including reductive alkylations with fluorinated benzaldehyde, [53] however, this is the first successful example of a radiosynthesis that leverages a radiofluorinated aliphatic aldehyde intermediate for subsequent reductive alkylation. The reductive alkylation reaction is chemoselective towards amines over alcohols, as opposed to nucleophilic substitution of an alkyl halide, where overalkylation of tertiary amines and alkylation of alcohols typically occur as side reactions. Boronic acid pinacol ester **3** was used as precursor for the radiosynthesis, as the copper-mediated radiofluorination of arylboronic esters constitutes a reliable and versatile labeling strategy. [54] Arylboronic esters as precursors

can be readily obtained by Miyaura-borylation of aryl halides in one step. [55] In contrast to other established radio-precursors, oxidative conditions are not required (cf. diaryliodonium salts or iodonium ylides). [56, 57] Another advantage of copper-mediated radiofluorination of boronic acid esters is that regioselectivity issues during fluorine-18 incorporation are not typically observed, as opposed to the radiofluorination of diaryliodonium salts. [58]

Boronic acid pinacol ester **3** (Scheme 1), which served as precursor for the radiolabeling, was obtained in a multistep synthesis, starting from commercially available 1iodo2halobenzenes **6a–c**. A Heck reaction [59] with but-3-en-1-ol, followed by isomerization, [60, 61] gave aldehydes **7a–c** in variable yields and purity (Scheme 2). Indeed, only in the case of 1,2diidodobenzene, the reaction led to pure 4(2iodophenyl)butanal (**7a**). In sharp contrast, the bromo and fluoro analogues, **6b** and **6c**, yielded inseparable mixtures of 4(2halophenyl)butanal (**7b** and **7c**) and undesired regioisomers 3(2haloophenyl)butanal (**8b** and**8c**, 10–11 %, from $^{1}$H NMR spectra analysis). Thus, despite the low yeld of 11 %, the synthesis was continued with **7a**. Aldehyde 7c was used as a non-radioactive reference for HPLC method development.

Protection of the aldehyde as an acetal (**9**) [62] was necessary, as the Miyaura-borylation gave only trace amounts of precursor **3**, when the reaction was performed directly with aldehyde **7a** (Scheme 3). With acetal **9**, the borylation [63] proceeded in 48% yield, followed by hydrolysis [64] to the pinacol precursor **3** in 91%. With an open-chain diethyl acetal, instead of cyclic ethylene acetal, the hydrolysis of the diethyl acetal required only very mild conditions using catalytic iodine in acetone. Thus, the diethyl acetal **9** ensured the successful Miyaura-borylation and allowed the facile release of the aldehyde functionality, while leaving the boronic ester intact. Accordingly, precursor **3** for the radiosynthesis was synthesized from 1,2diiodobenzene in four steps in an overall yield of %.

The racemic 3-benzazepine building block (*rac*)-**5** was obtained from commercially available 3-benzazepine **11** by cleavage of the benzyl ether via catalytic hydrogenation in 91% yield (Scheme 3). Chiral resolution of 3-benzazepine (*rac*)**-11** or (*rac*)**-5** to obtain enantiomerically pure 3-benzazepines (*R*)-**5** and (*S*)-**5** by chiral HPLC was not successful, using both normal and reversed stationary phases and various eluent combinations. Based on previous experience with this class of compounds, chiral resolution was generally possible for tertiary amines bearing a bulky lipophilic substituent. [39] Therefore, 3-benzazepine **11** was reductively *N*-alkylated with benzaldehyde and $NaBH(OAc)_3$ to give the tertiary amine (*rac*)-**12** in 99% yield. It is worthwhile mentioning that the benzyl group was selected to enable simultaneous cleavage of both, the benzyl ether and benzylamine after chiral resolution. Indeed, benzylated 3-benzazepines (*R*)-**12** and (*S*)**12** were successfully separated by chiral HPLC and the enantiomerically pure benzazepine building blocks (*R*)-**5** and (*S*)-**5** were obtained by catalytic hydrogenation of (*R*)-**12** and (*S*)-**12**, respectively.

The radiolabeling was performed using a two-step procedure involving copper-mediated nucleophilic radiofluorination of precursor **3**, [54] followed by reductive alkylation with the 3-benzazepine building blocks (*rac*)-, (*R*)- and (*S*)-**5**. A summary of radiochemical yields (RCYs), average synthesis time and molar

activities of (*rac*)-[$^{18}$F]OF-NB1, (*R*)-[$^{18}$F]OF-NB1 and (*S*)-[$^{18}$F]OF-NB1 is provided in Table 1. It should be noted that attempts to perform the reductive amination prior to the copper-mediated fluorine-18 labeling did not yield the desired product, potentially owing to the interference of the two alcohol groups (**Supporting Information**).

Table 1
Radiochemical yields (RCY), average synthesis time and molar activity of the radiosynthesis of (*rac*)-[$^{18}$F]OF-NB1, (*R*)-[$^{18}$F]OF-NB1 and (*S*)-[$^{18}$F]OF-NB1.

| Cmpd | RCY (d.c.) [%] | Molar activity [GBq/µmol] | Avg. time [min] | Radiochemical purity |
|---|---|---|---|---|
| (*rac*)-[$^{18}$F]OF-NB1 | 15 ± 5 (n = 6) | 8.4 (n = 2) | 97 ± 12 (n = 6) | > 99% |
| (*R*)-[$^{18}$F]OF-NB1 | 15 (n = 2) | 13.6 (n = 2) | 120 (n = 2) | > 99% |
| (*S*)-[$^{18}$F]OF-NB1 | 15 (n = 2) | 10.2 (n = 2) | 114 (n = 2) | > 99% |

RCY: radiochemical yield; n.d.c.: non-decay corrected; d.c.: decay corrected.

In vitro **autoradiography with rodent brain tissue**

GluN2B subunit-specificity and selectivity of (*R*)-[$^{18}$F]OF-NB1 and (*S*)-[$^{18}$F]OF-NB1 were assessed by *in vitro* autoradiography using mouse and rat brain tissue sections. In accordance with reported GluN2B expression patterns in the adult mammalian brain, [65] a high tracer binding was observed in GluN2B-rich forebrain regions such as the hippocampus, striatum, thalamus and cortex, whereas tracer binding was relatively low in the GluN2B-deficient cerebellum (Fig. 1). Although the latter observations were generally made for both enantiomers, (*R*)-[$^{18}$F]OF-NB1 exhibited a more favorable binding pattern in the rodent brain (Fig. 1A), which was superior to that of (*S*)-[$^{18}$F]OF-NB1 (Fig. 1B) with respect to selectivity for GluN2B-rich brain areas. In concert with these observations, blocking studies with the commercially available GluN2B antagonist, CP101,606 ($K_D$ of 10 nM towards GluN2B), revealed a more pronounced reduction of tracer binding for (*R*)-[$^{18}$F]OF-NB1 as compared to (*S*)-[$^{18}$F]OF-NB1 on mouse and rat brain sections.

One of the major drawbacks of previously reported GluN2B PET radioligands was off-target binding towards sigma receptors. [39] While we have previously demonstrated the *in vitro* and *in vivo* selectivity of (*rac*)-[$^{18}$F]OF-NB1 over sigma1 receptors; [44] it remains unclear whether off-target activity towards sigma2 receptors can also be excluded. As such, we performed additional autoradiography studies by challenging (*R*)-[$^{18}$F]OF-NB1 and (*S*)-[$^{18}$F]OF-NB1 with the previously reported sigma2 ligand, **11b**[66] (here

codenamed FA10, $K_i$ of 1.4 nM towards sigma2). Overall, no considerable signal reduction was observed for either (*R*)-[$^{18}$F]OF-NB1 or (*S*)-[$^{18}$F]OF-NB1 when employing an excess of FA10 (10 µM), indicating that both enantiomers exhibited selectivity over sigma2 receptors (Fig. 1).

Quantification of the autoradiographic data corroborated that highest (*R*)-[$^{18}$F]OF-NB1 binding was observed in the hippocampus, followed by the cortex, striatum and thalamus, whereas the cerebellum showed lowest (*R*)-[$^{18}$F]OF-NB1 binding (Fig. 2A) – with a hippocampus-to-cerebellum ratio of ≈ 20. Although similar quantification patterns were obtained for (*S*)-[$^{18}$F]OF-NB1 (Fig. 2B), the hippocampus-to-cerebellum ratio was ≈ 5, indicating that the selectivity for the GluN2B-rich forebrain was less accentuated. While GluN2B blockade studies with CP101606 showed a significant signal reduction, which was more pronounced for (*R*)-[$^{18}$F]OF-NB1 (96% signal reduction) than for (*S*)-[$^{18}$F]OF-NB1 (85% signal reduction), sigma2 blockade with FA10 did not reveal a significant signal reduction in the hippocampus for both tracer enantiomers. These results indicated that (*R*)-[$^{18}$F]OF-NB1 exhibits a higher specificity and selectivity for the GluN2B subunit than (*S*)-[$^{18}$F]OF-NB1 *in vitro*.

## PET imaging and in vivo blocking studies

In a next step, we sought to assess the *in vivo* performance characteristics of (*R*)-[$^{18}$F]OF-NB1 and (*S*)-[$^{18}$F]OF-NB1 by small animal PET imaging. Upon tail-vein injection to CD1 mice, brain uptake was determined by visual inspection of the images as well as by quantification of volumes of distribution ($V_T$) across different brain regions. As depicted in Fig. 3, (*R*)-[$^{18}$F]OF-NB1 exhibited a higher overall uptake in the rodent brain than (*S*)-[$^{18}$F]OF-NB1.

These findings were corroborated by quantification of $V_T$ across different brain regions using Logan plot analyses [67], where we found significantly higher $V_T$ values for (*R*)-[$^{18}$F]OF-NB1 than for (*S*)-[$^{18}$F]OF-NB1 in the whole brain, as well as in GluN2B-rich brain regions (Fig. 4A). These findings indicated a higher retention of the *R*-enantiomer in the rodent brain. Notable, blockade experiments with sigma2 ligand, FA10 (1 mg/kg), did not result in a significant reduction of the PET signal in the hippocampus (Fig. 4B), or in any other brain region (data not shown), indicating that both enantiomers were selective over sigma2 receptors *in vivo*.

## In vitro autoradiography with non-human primate brain sections

Due to the superior performance characteristics of (*R*)-[$^{18}$F]OF-NB1 in rodent studies, we sought to assess its utility for imaging GluN2B subunit-containing NMDA receptors in higher species. As such, post-mortem brain tissue sections from non-human primates (NHPs) were used for autoradiographic testing of (*R*)-[$^{18}$F]OF-NB1. In accordance with observations from rodent studies, we found a heterogenous binding pattern with preferential accumulation of (*R*)-[$^{18}$F]OF-NB1 in GluN2B-rich brain regions (Fig. 5). Employing GluN2B antagonist, CP101,606, a high degree of specificity (80.7% signal reduction) was corroborated. In

contrast, blockade studies with FA10 did not reveal a significant reduction of the signal, implying that (*R*)-[$^{18}$F]OF-NB1 is selective over sigma2 receptors in NHPs.

# Conclusion

In the present study, we developed a novel synthetic strategy to obtain enantiomerically pure (*R*)-[$^{18}$F]OF-NB1 and (*S*)-[$^{18}$F]OF-NB1, thereby circumventing the previously reported use of corrosive reagents and allowing for method translation to human-grade production facilities. (*R*)-[$^{18}$F]OF-NB1 significantly outperformed (*S*)-[$^{18}$F]OF-NB1 in autoradiographic experiments using mouse and rat brain, in particular, by exhibiting a higher specificity and selectivity for GluN2B-rich brain regions. While both enantiomers were selective over sigma2 receptors *in vitro* and *in vivo*, small animal PET experiments revealed higher volumes of distribution for (*R*)-[$^{18}$F]OF-NB1 in GluN2B-rich regions of the rodent brain. Overall, these findings suggest that (*R*)-[$^{18}$F]OF-NB1 constitutes a promising GluN2B-targeted PET radioligand for clinical translation.

# Experimental Section

Reagents and solvents were purchased from Sigma-Aldrich, Fisher Scientific, TCI, Combi-Blocks or Labnetwork Inc and were used without further purification. Solvents used in radiosynthesis were purchased in anhydrous grade (puriss., dried over molecular sieves, $H_2O < 0.005\%$), solvents necessary for extractions, column chromatography and thin-layer chromatography (TLC) were acquired as technical grade. Anhydrous solvents needed for conventional organic synthesis were obtained by drying over molecular sieve (4 Å) under nitrogen atmosphere. Nonaqueous reactions were generally performed under nitrogen atmosphere using flame-dried glassware and standard syringe/septa methods. Reactions were magnetically stirred and further monitored by TLC performed on Merck TLC glass sheets (silica gel 60 $F_{254}$). TLC Spots were visualized with UV light ($\lambda$ = 254 nm). Chromatographic purification of products was performed using a Biotage® Selekt System with Biotage® Sfär columns. Reactions at 0°C were carried out using an ice/water bath for cooling purposes. $^1$H and $^{13}$C NMR spectra were recorded on a Bruker Ascend 600 MHz spectrometer and the chemical shifts ($\delta$) are presented in ppm referenced to tetramethylsilane (0 ppm). Analysis of NMR spectra was performed with the MestReNova software (14.2.0). All coupling constants (*J*) are reported in Hz. Multiplicities in the $^1$H NMR spectra are generally given as either s, singlet; d, doublet; dd, doublet of doublets; t, triplet; dt, doublet of triplets; m, multiplet; or bs, broad singlet. High-resolution mass spectrometry (HRMS) was conducted on a ThermoFisher Scientific Exactive™ Plus Orbitrap Mass Spectrometer, using atmospheric pressure chemical ionization (APCI) in the positive ionization mode; the resulting data is reported in *m/z*. Melting points were determined with a Mel-Temp® capillary melting point apparatus. The radioactivity of samples was quantified with a Capintec CRC®-15R radioisotope dose calibrator. Reaction progress in radiochemistry was monitored with Eckert & Ziegler AR-2000 radio-TLC imaging scanner, operated with the WinScan software (3.14). Purification of the radiotracers was performed on a semipreparative HPLC with a Merck Hitachi LaChrome L-7100 pump system, a Shimadzu SPD-10AV UV-vis detector and a Carroll & Ramsey

Associates Model 105-S radiation detector, operated with the PowerChrom software (2.7.9). The semipreparative column used was a Venusil MP C18 (10 mm × 250 mm, 5 µm) with an isocratic eluent mixture of water and $CH_3CN$ (v/v = 65:35, + 0.1% trifluoroacetic acid (TFA)), a flow rate of 5 mL/min for 15 min and UV detection at 254 nm. For quality control, an aliquot of the final formulation of radiotracer was analysed by analytical HPLC, using a LabAlliance Series III pump system, Waters 2487 Dual λ Absorbance Detector UV-vis detector, Carroll & Ramsey Associates Model 105-S radiation detector, operated with the PowerChrom software (2.7.9). The analytical column used was XBridge™ Phenyl (4.6 mm × 100 mm, 3.5 µm) with an isocratic mixture of water and $CH_3CN$ (v/v = 75:25, + 0.1% TFA), a flow rate of 1 mL/min for 25 min ($t_R$ = 15.9 min) and UV detection at 254 nm. The molar activity of radiotracers was determined by comparing the UV intensity of a sample of the formulated product of known activity, against a calibration curve of the corresponding cold reference of known concentration. The calibration curve was determined from injecting a sample of 80 µL of OF-NB1 solutions in HPLC eluent in six concentrations between 0.1 mg/L and 0.0005 mg/L into the analytical HPLC and measuring the area under the curve of the corresponding UV signal (cf. **Supporting Information**). Animals were purchased from Charles River or Jackson Laboratory and kept under standard conditions. All animal studies were approved and carried out in accordance with the Institutional Animal Care and Use Committee (IACUC) guidelines.

# Chemistry

# General procedure for the synthesis of 4-(2-halophenyl)butanal 7a–7c

A flame dried Schlenk flask was charged with $Pd(OAc)_2$ (6 mol%), tetrabutylammonium bromide (1.00 eq.), $NaHCO_3$ (2.50 eq.) and molecular sieves (4 Å). The air atmosphere was exchanged by nitrogen in three cycles of evacuation and flushing with $N_2$. The reagents were suspended in DMF (dry), the iodohaloaryl compound (**6a**–**6c**, 1.00 eq.) was dissolved in DMF (dry) and added to the mixture. But-3-en1ol was added and the mixture was stirred at 70°C for 4 h. After cooling down, ethyl acetate was added, and the mixture was filtered through a pad of Celite®. It was washed with water and the aqueous layer was extracted with ethyl acetate, the organic layers were combined and concentrated *in vacuo*. This process was repeated two more times. The organic layer was dried with $Na_2SO_4$ and evaporated *in vacuo*. The crude product was purified via flash column chromatography to yield product **7a**–**c**.

# 4-(2-Iodophenyl)butanal (7a)

Following the general procedure for the synthesis of 4-(2-halophenyl)butanal, $Pd(OAc)_2$ (280 mg, 1.25 mmol, 6 mol%), tetrabutylammonium bromide (6.71 g, 20.8 mmol, 1.00 eq.), $NaHCO_3$ (4.47 g, 52.0 mmol, 2.50 eq.) and molecular sieves (4 g) were suspended in DMF (60 mL), 1,2diiodobenzene (**6a**, 6.86 g, 20.8 mmol, 1.00 eq.) was dissolved in DMF (15 mL) and added with but-3-en1ol (1.50 g, 20.8 mmol, 1.00 eq.) to the mixture. After cooling down, ethyl acetate (100 mL) was added and after filtration it was washed

with water (300 mL) and the aqueous layer was extracted with ethyl acetate (3 × 100 mL). The residue was purified via flash column chromatography (hexanes/ethyl acetate = 1:0 → 95:5). Yellow oil, yield 639 mg (2.33 mmol,11 %). TLC: 0.39 (hexanes/ethyl acetate = 9:1). $^{1}$H NMR (600 MHz, DMSO-$d_6$): $\delta$ (ppm) = 1.81 (quint d, $J$ = 7.6/1.6 Hz, 2H, C$H_2$CH$_2$CHO), 2.47–2.54 (m, 2H, C$H_2$CHO), 2.68 (t, $J$ = 7.6 Hz, 2H, C$H_2$CH$_2$CH$_2$CHO), 6.97 (td, $J$ = 7.6/1.8 Hz, 1H, 5-H$_{iodophenyl}$), 7.31 (d, $J$ = 7.7 Hz, 1H, 3-H$_{iodophenyl}$), 7.35 (t, $J$ = 7.2 Hz, 1H, 4-H$_{iodophenyl}$), 7.83 (d, $J$ = 7.9 Hz, 1H, 6-H$_{iodophenyl}$), 9.67–9.72 (m, 1H, CHO). $^{13}$C NMR (151 MHz, DMSO-$d_6$): $\delta$ (ppm) = 22.3 (1C ,$C$H$_2$CH$_2$CHO), 39.1 (1C, $C$H$_2$CH$_2$CH$_2$CHO), 42.3 (1C, $C$H$_2$CHO), 100.7 (1C, C-1$_{iodophenyl}$), 128.3 (1C, C-5$_{iodophenyl}$), 128.6 (1C, C4$_{iodophenyl}$), 129.7 (1C, C-3$_{iodophenyl}$), 139.1 (1C, C-6$_{iodophenyl}$), 143.9 (1C, C-2$_{iodophenyl}$), 203.1 (1C, CHO). HRMS: $m/z$ = 256.9820, calcd. 256.9822 for $C_{10}H_{10}I^{+}$ [M + H-H$_2$O]$^{+}$.

# 4-(2-Bromophenyl)butanal (7b) / 3-(2-bromophenyl)butanal (8b)

Following the general procedure for the synthesis of 4-(2-halophenyl)butanal, Pd(OAc)$_2$ (40.4 mg, 180 µmol, 6 mol%), tetrabutylammonium bromide (967 mg, 3.00 mmol, 1.00 eq.), NaHCO$_3$ (630 mg, 7.50 mmol, 2.50 eq.) and molecular sieves (600 mg) were suspended in DMF (10 mL), 1-iodo-2-bromobenzene (**6b**, 849 mg, 3.00 mmol, 1.00 eq.) was dissolved in DMF (2 mL) and added with but-3-en1ol (325 mg, 4.5 mmol, 1.50 eq.) to the mixture. After cooling down, ethyl acetate (10 mL) was added, after filtration it was washed with water (50 mL) and the aqueous layer was extracted with ethyl acetate (3 × 50 mL). The crude product was purified via flash column chromatography (hexanes/ethyl acetate = 1:0 → 9:1) and yielded the product **7b** as a yellow oil (521 mg, 2.29 mmol, 6 %), containing about 0 % of undesired regioisomer 3-(2-bromophenyl)butanal (**8b**). TLC: 0.40 (hexanes/ethyl acetate = 9:1). $^{1}$H NMR (600 MHz, DMSO-$d_6$): $\delta$ (ppm) = 1.19* (d, $J$ = 6.2 Hz, 0.3H, CH$_3$), 1.77–1.88 (m, 2H, CH$_2$), 2.46–2.52 (m, 1.8H, CH$_2$), 2.65–2.72 (m, 1.8H, CH$_2$), 2.76–2.86* (m, 0.2H, CH$_2$), 3.69* (h, $J$ = 7.0 Hz, 0.1H, C$H$CH$_3$), 7.13–7.17 (m, 0.9H, 5-H$_{bromophenyl}$), 7.30–7.36 (m, 1.8H, 3/4-H$_{bromophenyl}$), 7.56–7.60 (m, 0.9H, 6-H$_{bromophenyl}$), 9.63–9.64* (m, 0.1H, CHO), 9.67–9.68 (m, 0.9H, CHO). * indicates observed isolated proton signals of regioisomer 3(2bromophenyl)butanal in relative intensity of 10%. HRMS: $m/z$ = 208.9962, calcd. 208.9960 for $C_{10}H_{10}{}^{79}Br^{+}$ [M + H-H$_2$O]$^{+}$.

# 4-(2-Fluoroophenyl)butanal (7c) / 3-(2-fluorophenyl)butanal (8c)

Following the general procedure for the synthesis 4-(2-halophenyl)butanal, Pd(OAc)$_2$ (40.4 mg, 180 µmol, 6 mol%), tetrabutylammonium bromide (967 mg, 3.00 mmol, 1.00 eq.), NaHCO$_3$ (630 mg, 7.50 mmol, 2.50 eq.) and molecular sieves (600 mg) were suspended in DMF (10 mL), 1-iodo-2-fluorobenzene (**6c**, 666 mg, 3.00 mmol, 1.00 eq.) was dissolved in DMF (2 mL) and added with but-3-en1ol (324 mg, 4.5 mmol, 1.50 eq.) to the mixture. After cooling down, ethyl acetate (10 mL) was added, after filtration it was washed with water (50 mL) and the aqueous layer was extracted with ethyl acetate (3 × 50 mL). The crude product was purified via flash column chromatography (hexanes/ethyl acetate = 1:0 → 9:1) and yielded

the product **7c** as a yellow oil (351 mg, 2.11 mmol, 0 %), containing about 1 % of the undesired regioisomer 3-(2-fluorophenyl)butanal (**8c**). TLC: 0.43 (hexanes/ethyl acetate = 9:1). $^1$H NMR (600 MHz, DMSO-$d_6$): $\delta$ (ppm) = 1.21* (d, $J$ = 7.0 Hz, 0.33H, $CH_3$), 1.81 (p, $J$ = 7.6 Hz, 1.78H, $CH_2$), 2.46 (td; $J$ = 7.3, 1.5 Hz; 1.78H; $CH_2$), 2.61 (t, $J$ = 7.7 Hz, 1.78H, $CH_2$), 2.72–2.85* (m, 0.22H, $CH_2$), 3.57* (h, $J$ = 7.1 Hz, 0.11H, C*H*$CH_3$), 7.10–7.16 (m, 1.78H, aryl), 7.22–7.27 (m, 0.89H, aryl), 7.29 (td; $J$ = 7.7, 1.8 Hz; 0.89H; aryl), 7.35* (td; $J$ = 7.9, 1.9 Hz; 0.11H; aryl), 9.62* (t, $J$ = 1.7 Hz, 0.11H, CHO), 9.66 (t, $J$ = 1.5 Hz, 0.89H, CHO). * indicates isolated proton signals of regioisomer 3(2fluorophenyl)butanal in relative intensity of 11%. HRMS: $m/z$ = 149.0762., calcd. 149.0761for $C_{10}H_{10}F^+$ $[M + H\text{-}H_2O]^+$.

# 4-(2-Iodophenyl)butanal diethyl acetal (9)

4-(2-iodophenyl)butanal (**7a**, 600 mg, 2.19 mmol, 1.00 eq.), ethanol (510 µL, 8.76 mmol, 4.00 eq.) and *p*-toluenesulfonic acid monohydrate (83 mg, 0.44 mmol, 0.20 eq.) were dissolved in hexanes at 0°C. Molecular sieves (400 mg) were added and the mixture was stirred at 0°C. After 30 min, a second portion of *p*-toluenesulfonic acid monohydrate (83 mg, 0.44 mmol, 0.20 eq.) was added, together with additional molecular sieves (200 mg) and the mixture was stirred for further 20 min at 0°C. The mixture was filtered over a pad of cotton, which was extracted with hexanes and ethyl acetate (10 mL each). The solvent was evaporate*d in vacuo* and the residue was purified via flash column chromatography (hexanes/ethyl acetate = 1:0 → 95:5). and yielded the product **9** as a yellow oil (591 mg, 1.70 mmol, 78%), which was directly used for the subsequent reaction. TLC: 0.50 (hexanes/ethyl acetate = 95:5).

# 4-[2-(4,4,5,5-Tetramethyl-1,3,2-dioxaborolan-2-yl)phenyl]butanal diethyl acetal (10)

A flame dried Schlenk flask was charged with bis(pinacolato)diboron (802 mg, 3.16 mmol, 2.00 eq.), Pd(dppf)$Cl_2$ (69.3 mg, 94.8 µmol, 6 mol%) and KOAc (543 mg, 5.53 mmol, 3.50 eq.). The air atmosphere was exchanged by $N_2$ in three cycles of evacuation and flushing with nitrogen. After suspending the mixture in DMF (15 mL, dry) and adding iodoacetal **9** (550 mg, 1.58 mmol, 1.00 eq.) dissolved in DMF (5 mL, dry), the reaction mixture was stirred at 80°C for 4 h. After cooling down, the mixture was diluted with ethyl acetate (30 mL) and filtered over a pad of Celite®. The mixture was concentrated *in vacuo*, diluted with $H_2O$ (100 mL) and extracted with ethyl acetate (3 × 50 mL). The organic layers were combined and concentrated *in vacuo* and the extraction procedure was repeated two more times. The combined organic layers were dried over $Na_2SO_4$ and the solvent was removed under reduced pressure. The residue was purified via flash column chromatography (hexanes/ethyl acetate = 1:0 → 95:5) and yielded the product **10** as a yellow oil (264 mg, 758 µmol, 48%), which was directly used for the subsequent reaction. TLC: 0.48 (hexanes/ethyl acetate = 9:1).

# 4-(2-(4,4,5,5-Tetramethyl-1,3,2-dioxaborolan-2-yl)phenyl)butanal (3)

Diethyl acetal **10** (240 mg, 693 µmol, 1.00 eq.) and iodine (18 mg, 69 µmol, 0.10 eq.) were dissolved in acetone (2.5 mL) which was prior dried over $Na_2SO_4$. The reaction mixture was stirred at rt for 40 min. The mixture was diluted with ethyl acetate (20 mL) and washed with half concentrated aqueous $Na_2SO_3$ solution (20 mL). The aqueous layer was extracted with ethyl acetate (20 mL) and the combined organic layers were dried over $Na_2SO_4$ and the solvent was removed *in vacuo*. The residue was purified via flash column chromatography (hexanes/ethyl acetate = 97:3 → 94:6). Yellow oil, yield 172 mg (628 µmol, 91%). TLC: 0.38 (hexanes/ethyl acetate = 9:1). $^1$H NMR (600 MHz, $CDCl_3$): $\delta$ = 1.34 (s; 12H; $CH_3$), 1.92 (p; $J$ = 7.4 Hz; 2H; C$H_2$CH$_2$CHO), 2.44 (td; $J$ = 7.3, 2.0 Hz; 2H; C$H_2$CHO), 2.89–2.97 (m; 2H; C$H_2$CH$_2$CH$_2$CHO), 7.17 (d; $J$ = 7.7 Hz; 1H; 6-H$_{phenylalkyl}$), 7.20 (td; $J$ = 7.4, 1.2 Hz; 1H; 4-H$_{phenylalkyl}$), 7.36 (td; $J$ = 7.5, 1.6 Hz; 1H; 5-H$_{phenylalkyl}$), 7.80 (dd; $J$ = 7.4, 1.6 Hz; 1H; 3-H$_{phenylalkyl}$), 9.77 (t; $J$ = 2.0 Hz; 1H; CHO). $^{13}$C NMR (151 MHz, $CDCl_3$): $\delta$ = 25.0 (4C, $CH_3$), 25.7 (1C; C$H_2$CH$_2$CHO), 35.1 (1C; C$H_2$CH$_2$CH$_2$CHO), 43.6 (1C; C$H_2$CHO), 83.7 (2C; C(CH$_3$)$_2$), 125.5 (1C; C4$_{phenylalkyl}$), 129.5 (1C; C-6$_{phenylalkyl}$), 131.2 (1C; C5$_{phenylalkyl}$), 136.5 (1C; C-3$_{phenylalkyl}$), 148.6 (1C, C-1$_{phenylalkyl}$), 203.2 (1C, CHO), C-2$_{phenylalkyl}$ was not observed. HRMS: $m/z$ = 275.1813., calcd. 275.1813 for $C_{16}H_{24}O_3B^+$ $[M + H]^+$.

### (rac)-2,3,4,5-Tetrahydro-1H-3-benzazepine-1,7-diol ((rac)-5)

A flask was charged with 3-benzazepine **11** (500 mg, 1.86 mmol, 1.00 eq.) and Pd/C (200 mg, 10 wt%) and THF (25 mL) was added. The air atmosphere was exchanged with a hydrogen atmosphere, by flushing the flask with $H_2$ for 10 min. A balloon with $H_2$ was connected to the flask and the reaction mixture was stirred at 60°C overnight. After cooling down, the mixture was filtered over Celite® and the filter was extracted with MeOH (6 × 30 mL). The solvent was removed *in vacuo.* Beige solid, mp 173°C (decomposition), yield 303 mg (1.69 mmol, 91%). $^1$H NMR (600 MHz, DMSO-$d_6$): $\delta$ (ppm) = 2.56–2.68 (m, 3H, 2-H, 4-H, 5-H), 2.75–2.81 (m, 1H, 4-H), 2.82–2.88 (m, 2H, 2-H, 5-H), 4.48 (d, $J$ = 7.5 Hz, 1H, 1-H), 5.08 (bs, 1H, CHO*H*), 6.46 (d; $J$ = 2.5 Hz; 1H, 2-H), 6.49 (dd, $J$ = 8.1/2.5 Hz, 1H, 6-H), 7.11 (d, $J$ = 8.2 Hz, 1H; 5-H), 9.13 (bs, 1H, PhOH). A signal for the NH proton is not observed in the spectrum. $^{13}$C NMR (151 MHz, DMSO-$d_6$): $\delta$ (ppm) = 39.6 (1C, C-5), 48.1 (1C, C-4), 55.5 (1C, C-2), 73.7 (1C, C-1), 111.5 (1C, C-6), 116.5 (1C, C-2), 127.2 (1C, C-5), 135.4 (1C, C-4), 141.3 (1C, C-3), 155.6 (1C, C-1). HRMS: $m/z$ = 162.0914., calcd. 162.0913 for $C_{10}H_{12}NO^+$ $[m + H\text{-}H_2O]^+$.

### (rac)-3-Benzyl-7-(benzyloxy)-2,3,4,5-tetrahydro-1H-3-benzazepin-1-ol ((rac)-12)

3-Benzazepine (*rac*)-**11** (100 mg, 371 µmol, 1.00 eq.) and benzaldehyde (45 µL, 0.45 mmol, 1.2 eq.) were suspended in THF (5 mL, dry). Under stirring, NaBH(OAc)$_3$ (197 mg, 928 µmol, 2.50 eq.) was added at once and the mixture was stirred at rt overnight. An aqueous saturated $NH_4Cl$ solution (5 mL) and water (15 mL) were added and the mixture was extracted with ethyl acetate (3 × 20 mL). The combined organic layers were dried ($Na_2SO_4$) and the solvent was removed under reduced pressure. The residue was purified via flash column chromatography ($CH_2Cl_2$/$CH_3OH$ (+ 1% conc. $NH_{3\ aq.}$) = 99:1 → 90:10). Yellow viscous oil, yield 133 mg (370 µmol, 99%). $^1$H NMR (600 MHz, $CDCl_3$): $\delta$ (ppm) = 2.64–2.67 (m, 1H, 4-H),

2.78–2.83 (m, 2H, 5-H, 2-H), 3.10–3.13 (m, 1H, 4-H), 3.32–3.39 (m, 2H, 2-H, 5-H), 3.95 (s, 2H, PhC$H_2$N), 4.84 (d, $J$ = 7.0 Hz, 1H, 1-H), 5.02 (s, 2H, PhC$H_2$O), 6.70 (d, $J$ = 2.6 Hz, 1H; 2-$H_{phenoxy}$), 6.75 (dd, $J$ = 8.3/2.7 Hz, 1H, 6-$H_{phenoxy}$), 7.17 (d, $J$ = 8.3 Hz, 1H, 5-$H_{phenoxy}$), 7.29–7.43 (m, 10H, $H_{benzyl}$). $^{13}$C NMR (151 MHz, $CDCl_3$): $\delta$ (ppm) = 34.9 (1C, C-5), 55.1 (1C, C-4), 60.2 (C-2), 63.6 (1C, PhC$H_2$N), 70.1 (1C, Ph$C$H$_2$O), 71.3 (1C, C-1), 111.7 (1C, C6$_{phenoxy}$), 117.3 (1C, C-2$_{phenoxy}$), 127.6 (2C, C-2/6$_{benzoxyl}$), 128.1 (1C, C4$_{benzoxy/benzaminyl}$), 128.6 (1C, C-4$_{benzoxyl/benzaminyl}$), 128.7 (2C, C-3/5$_{benzoxyl/benzaminyl}$), 128.9 (2C, C-3/5$_{benzoxyl/benzaminyl}$), 129.4 (1C, C-5$_{phenoxy}$), 130.2 (2C, C-2/6$_{benzaminyl}$), 134.6 (1C, C-4$_{phenoxy}$/C-1$_{benzaminyl}$), 134.9 (1C, C-4$_{phenoxy}$/C-1$_{benzaminyl}$), 137.0 (1C, C1$_{benzoxyl}$), 140.3 (1C, C-3$_{phenoxy}$), 158.4 (1C, C-1$_{phenoxy}$). HRMS: $m/z$ = 360.1955., calcd. 360.1958 for $C_{24}H_{26}NO_2^+$ $[m + H]^+$.

### Separation of (R)- and (S)-3-benzyl-7-(benzyloxy)-2,3,4,5-tetrahydro-1H-3-benzazepin-1-ol ((R)-/(S)-12)

Enantiomeric purification of (*rac*)-**12** was performed by semi-preparative HPLC with an Agilent 1260 Inifinity II system, operated with the OpenLab ChemStation software, and a normal phase ReproSil Chiral-NR (8 µm, 250mm × 10 mm) column using an isocratic eluent mixture of hexanes and isopropanol (v/v = 8:2), with a flowrate of 5 mL/min for 40 min and UV detection at 210 and 250 nm. Racemic **12** (80 mg) was dissolved in a mixture of hexanes and isopropanol (15 mL, v/v = 2:1). The separation was performed in three injections with each 5 mL of this solution. The (*S*)-enantiomer eluted first with a retention time of 9.1 min and was isolated as colorless oil, yield 36.2 mg (91%). The (*R*)-enantiomer eluted second with a retention time of 24.5 min and was isolated as viscous colorless oil, yield 39.8 mg (99%). Enantiomeric purity was determined by injecting a sample of separated (*R*)-**12** and (*S*)-**12**, respectively into the HPLC system. The corresponding chromatograms are shown in the **Supporting Information**.

### (R)-2,3,4,5-Tetrahydro-1H-3-benzazepine-1,7-diol ((R)-5)

(*R*)-**12** (39.8 mg, 111 µmol) was dissolved in THF (5 mL, dry) and Pd/C (10 mg, 10 wt%) was added. The air atmosphere was exchanged with a hydrogen atmosphere, by flushing the flask with $H_2$ for 10 min. A balloon with $H_2$ was connected to the flask and the reaction mixture was stirred at 60°C overnight. After cooling down, the solvent was removed *in vacuo* and the residue was suspended in $CH_3OH$ (10 mL) and passed through a syringe filter. The solvent was removed under reduced pressure and the residue was suspended in ethyl acetate (5 mL) and passed through a pad of cotton and washed with ethyl acetate. The residue on the filter was dissolved in $CH_3OH$ and passed through the filter. The solvent was removed *in vacuo*. Colorless solid, yield 9.7 mg (54 µmol, 49%). The analytical data are in agreement with the data of (*rac*)-**5**.

### (S)-2,3,4,5-Tetrahydro-1H-3-benzazepine-1,7-diol ((S)-5)

(*S*)-X (36.2 mg, 101 µmol) was reacted and worked-up as described above for (*R*)-X. Colorless solid, yield 11.7 mg (65.3 µmol, 65%). The analytical data are in agreement with (*rac*)-**5**.

# Radiochemistry

[$^{18}$F]Fluoride ions were produced by bombardment of 98% enriched [$^{18}$O]$H_2O$ via the $^{18}O(p,n)^{18}F$ nuclear reaction. Aqueous [$^{18}$F]fluoride was trapped on a preconditioned anion-exchange cartridge (Waters Sep-Pak® Plus Light QMA, preconditioned with 10 mL sat. $NaHCO_{3\ aq}$. and 10 mL water).

For the building block approach, [$^{18}$F]fluoride was eluted with a solution of tetraethylammonium bicarbonate (TEAB) in methanol (1.5 mL, 1 mg/mL) into a reaction vial, followed by azeotropic drying with $CH_3CN$ (1 × 1 mL). Boronic ester **3** (2 mg) and $Cu(OTf)_2(py)_4$ (6 mg) were dissolved in 300 µL of a mixture of dry *N*,*N*dimethylacetamide (DMA) and dry *n*-BuOH (v/v = 2:1) and added into the reaction vial. The mixture reacted in the open vial at 110°C for 20 min. After cooling down, the mixture was diluted with water (8 mL) and passed through a C18-catridge (Waters Sep-Pak® Plus Light C18, preconditioned with 5 mL EtOH and 5 mL water), the cartridge was washed with water (5 mL) and thoroughly dried in air stream. The organic mixture trapped on the cartridge was eluted with dry DMF (0.5 mL) into a reaction vial charged with 3-benzazepine **5** (3 mg), $NaBH(OAc)_3$ (4.5 mg) and a stir bar, and the mixture was stirred at 60°C for 30 min. After cooling down, the mixture was diluted with 4 mL of a mixture of water/$CH_3CN$ (v/v = 65:35, + 0.1% TFA) and purified via semipreparative HPLC ($t_R$ = 10.0 min). The collected fractions were diluted with 30 mL of water and passed through an a C18 cartridge (Waters Sep-Pak® Plus Light C18, preconditioned with 5 mL EtOH and 5 mL water) and the cartridge was washed with water (5 mL). [$^{18}$F]OF-NB1 was eluted with EtOH (0.6 mL) from the cartridge into the final formulation vial. Radiochemical yields, average reaction times and molar activities are shown above in Table 1. Conditions for the single step radiosynthesis approach can be found in the **Supporting Information**.

**I**n vitro **autoradiography**

In vitro autoradiography studies were performed as previously described, however, with minor modifications. [42] Tissue-TEK (O.C.T.) was utilized to embed rodent and NHP postmortem brain tissue, which was subsequently prepared as 20 µm thick tissue sections on a cryostat and mounted on glass slides. The slides were then stored at -80°C until the time of utilization. Brain sections were initially thawed for 10 min on ice prior to *in vitro* autoradiography experiments. They were then preconditioned for 10 min in the assay buffer (pH 7.4) composed of 30 mM HEPES, 0.56 mM $MgCl_2$, 110 mM NaCl, 5 mM KCl, 3.3 mM $CaCl_2$ and 1% fatty acid-free bovine serum albumin (BSA) at ambient temperature. The tissue sections were then dried and subsequently incubated for 30 min at room temperature with (*R*)- or (*S*)-[$^{18}$F]OF-NB1 solution, respectively. For blockade conditions, 10 µM of the respective blocker were added. These blockers included CP101606 (GluN2B ligand) and FA10 (sigma2 ligand). After incubation, the brain sections were washed in assay buffer for 5 minutes followed by washing buffer (same as assay buffer but without BSA) for 2 × 2 min. They were then dipped twice in distilled water for 5 seconds, subsequently dried and exposed to a phosphor imager plate for 180 min. The plates were scanned and on an Amersham Typhoon scanner, whereas ImageQuant TL 8.1 and ImageJ v1.53e were utilized for image analyses.

# PET imaging

PET imaging studies were performed under Institutional Animal Care and Use Committee (IACUC) guidelines. Female CD-1 mice (10–12 weeks of age) were kept under a 12-h light/12-h dark cycle, with ad libitum access to food and water. On the day of experiment, mice were scanned using a G8 PET scanner (Sofie) under 1–2% isoflurane in air/oxygen 1:1 anesthesia. Body temperature was monitored and maintained by a heating pad installed in the scanner bed. The tracer solution containing 0.6–1.5 MBq (*R*)- or (*S*)[$^{18}$F]OF-NB1 in 1 % ethanol and PBS (100–150 µL per mouse) was injected by use of preinstalled tail-vein catheter. Dynamic PET images were recorded for 60 minutes. For blocking experiments, intravenous injection of the sigma2-selective ligand, FA10 (1 mg/kg), dissolved in 1 % ethanol in PBS (50–100 µL), was performed shortly before tracer injection. PMOD (Zurich, Switzerland) software was used for the reconstruction of the dynamic PET images and volumes of interest were defined as previously described. [68] Volumes of distribution were determined by Logan plot analysis, using an image-derived arterial input function (IDIF) extracted from the heart blood pool of each animal, as previously described. [69, 70]

# Declarations


### Acknowledgement

This work was supported by the Research Training Group “Chemical biology of ion channels (Chembion)” funded by the Deutsche Forschungsgemeinschaft (DFG), which is gratefully acknowledged. We express our gratitude to the members of the Emory PET Imaging Center & Radiopharmaceutical Discovery Program, Department of Radiology and Imaging Sciences, Emory University School of Medicine, for their invaluable assistance. Furthermore, we gratefully acknowledge the financial support provided, in part, by NIH grants (MH117125, AG073428, AG075444 and AG080262). A.H. was supported by the Swiss National Science Foundation (SNSF).



### Author information

### Corresponding author information

*Email: ahmed.haider@usz.ch


### Conflict of interest

H.A, S.M.A and A.H. are co-founders of Nemosia AG and co-authors of the following patents: WO2020099537A1 and US2017224852A1.

# References

1. Traynelis, S. F.; Wollmuth, L. P.; McBain, C. J.; Menniti, F. S.; Vance, K. M.; Ogden, K. K.; Hansen, K. B.; Yuan, H.; Myers, S. J.; Dingledine, R., Glutamate receptor ion channels: structure, regulation, and function. Pharmacological reviews 2010, *62* (3), 405–96.
2. Regan, M. C.; Romero-Hernandez, A.; Furukawa, H., A structural biology perspective on NMDA receptor pharmacology and function. Current opinion in structural biology 2015, *33*, 68–75.
3. Reiner, A.; Levitz, J., Glutamatergic Signaling in the Central Nervous System: Ionotropic and Metabotropic Receptors in Concert. Neuron 2018, *98* (6), 1080–1098.
4. Paoletti, P.; Bellone, C.; Zhou, Q., NMDA receptor subunit diversity: impact on receptor properties, synaptic plasticity and disease. Nature reviews. Neuroscience 2013, *14* (6), 383–400.
5. Nowak, L.; Bregestovski, P.; Ascher, P.; Herbet, A.; Prochiantz, A., Magnesium gates glutamate-activated channels in mouse central neurones. Nature 1984, *307* (5950), 462–5.
6. Mayer, M. L.; Westbrook, G. L.; Guthrie, P. B., Voltage-dependent block by Mg2 + of NMDA responses in spinal cord neurones. Nature 1984, *309* (5965), 261–3.
7. Paoletti, P.; Neyton, J., NMDA receptor subunits: function and pharmacology. Current opinion in pharmacology 2007, *7* (1), 39–47.
8. Tang, Y. P.; Shimizu, E.; Dube, G. R.; Rampon, C.; Kerchner, G. A.; Zhuo, M.; Liu, G.; Tsien, J. Z., Genetic enhancement of learning and memory in mice. Nature 1999, *401* (6748), 63–9.
9. France, G.; Fernandez-Fernandez, D.; Burnell, E. S.; Irvine, M. W.; Monaghan, D. T.; Jane, D. E.; Bortolotto, Z. A.; Collingridge, G. L.; Volianskis, A., Multiple roles of GluN2B-containing NMDA receptors in synaptic plasticity in juvenile hippocampus. *Neuropharmacology* 2017, *112* (Pt A), 76–83.
10. Hanson, J. E.; Weber, M.; Meilandt, W. J.; Wu, T.; Luu, T.; Deng, L.; Shamloo, M.; Sheng, M.; Scearce-Levie, K.; Zhou, Q., GluN2B antagonism affects interneurons and leads to immediate and persistent changes in synaptic plasticity, oscillations, and behavior. Neuropsychopharmacology: official publication of the American College of Neuropsychopharmacology 2013, *38* (7), 1221–33.
11. von Engelhardt, J.; Doganci, B.; Jensen, V.; Hvalby, O.; Gongrich, C.; Taylor, A.; Barkus, C.; Sanderson, D. J.; Rawlins, J. N.; Seeburg, P. H.; Bannerman, D. M.; Monyer, H., Contribution of hippocampal and extra-hippocampal NR2B-containing NMDA receptors to performance on spatial learning tasks. Neuron 2008, *60* (5), 846–60.
12. Sanz-Clemente, A.; Nicoll, R. A.; Roche, K. W., Diversity in NMDA receptor composition: many regulators, many consequences. The Neuroscientist: a review journal bringing neurobiology, neurology and psychiatry 2013, *19* (1), 62–75.
13. Wenzel, A.; Fritschy, J. M.; Mohler, H.; Benke, D., NMDA receptor heterogeneity during postnatal development of the rat brain: differential expression of the NR2A, NR2B, and NR2C subunit proteins. Journal of neurochemistry 1997, *68* (2), 469–78.
14. Liu, X. B.; Murray, K. D.; Jones, E. G., Switching of NMDA receptor 2A and 2B subunits at thalamic and cortical synapses during early postnatal development. The Journal of neuroscience: the official journal of the Society for Neuroscience 2004, *24* (40), 8885–95.

15. Monyer, H.; Burnashev, N.; Laurie, D. J.; Sakmann, B.; Seeburg, P. H., Developmental and regional expression in the rat brain and functional properties of four NMDA receptors. Neuron 1994, *12* (3), 529–40.
16. Sheng, M.; Cummings, J.; Roldan, L. A.; Jan, Y. N.; Jan, L. Y., Changing subunit composition of heteromeric NMDA receptors during development of rat cortex. Nature 1994, *368* (6467), 144–7.
17. Seillier, C.; Lesept, F.; Toutirais, O.; Potzeha, F.; Blanc, M.; Vivien, D., Targeting NMDA Receptors at the Neurovascular Unit: Past and Future Treatments for Central Nervous System Diseases. International journal of molecular sciences 2022, *23* (18).
18. Parsons, M. P.; Raymond, L. A., Extrasynaptic NMDA receptor involvement in central nervous system disorders. Neuron 2014, *82* (2), 279–93.
19. Hynd, M. R.; Scott, H. L.; Dodd, P. R., Differential expression of N-methyl-D-aspartate receptor NR2 isoforms in Alzheimer's disease. Journal of neurochemistry 2004, *90* (4), 913–9.
20. Liu, J.; Chang, L.; Song, Y.; Li, H.; Wu, Y., The Role of NMDA Receptors in Alzheimer's Disease. Frontiers in neuroscience 2019, *13*, 43.
21. Gan, J.; Qi, C.; Mao, L. M.; Liu, Z., Changes in surface expression of N-methyl-D-aspartate receptors in the striatum in a rat model of Parkinson's disease. Drug design, development and therapy 2014, *8*, 165–73.
22. Zhang, Z.; Zhang, S.; Fu, P.; Zhang, Z.; Lin, K.; Ko, J. K.; Yung, K. K., Roles of Glutamate Receptors in Parkinson's Disease. International journal of molecular sciences 2019, *20* (18).
23. Tuo, Q. Z.; Zhang, S. T.; Lei, P., Mechanisms of neuronal cell death in ischemic stroke and their therapeutic implications. Medicinal research reviews 2022, *42* (1), 259–305.
24. Wu, Q. J.; Tymianski, M., Targeting NMDA receptors in stroke: new hope in neuroprotection. Molecular brain 2018, *11* (1), 15.
25. Qu, X. X.; Cai, J.; Li, M. J.; Chi, Y. N.; Liao, F. F.; Liu, F. Y.; Wan, Y.; Han, J. S.; Xing, G. G., Role of the spinal cord NR2B-containing NMDA receptors in the development of neuropathic pain. Experimental neurology 2009, *215* (2), 298–307.
26. Zhou, X. L.; Zhang, C. J.; Peng, Y. N.; Wang, Y.; Xu, H. J.; Liu, C. M., ROR2 modulates neuropathic pain via phosphorylation of NMDA receptor subunit GluN2B in rats. British journal of anaesthesia 2019, *123* (2), e239-e248.
27. Bliss, T. V.; Collingridge, G. L.; Kaang, B. K.; Zhuo, M., Synaptic plasticity in the anterior cingulate cortex in acute and chronic pain. Nature reviews. Neuroscience 2016, *17* (8), 485–96.
28. Samojedny, S.; Czechowska, E.; Panczyszyn-Trzewik, P.; Sowa-Kucma, M., Postsynaptic Proteins at Excitatory Synapses in the Brain-Relationship with Depressive Disorders. International journal of molecular sciences 2022, *23* (19).
29. Gerhard, D. M.; Wohleb, E. S.; Duman, R. S., Emerging treatment mechanisms for depression: focus on glutamate and synaptic plasticity. Drug discovery today 2016, *21* (3), 454–64.

30. Merchant, R. E.; Bullock, M. R.; Carmack, C. A.; Shah, A. K.; Wilner, K. D.; Ko, G.; Williams, S. A., A double-blind, placebo-controlled study of the safety, tolerability and pharmacokinetics of CP-101,606 in patients with a mild or moderate traumatic brain injury. Ann N Y Acad Sci 1999, *890*, 42–50.
31. Kemp, J. A.; McKernan, R. M., NMDA receptor pathways as drug targets. Nature neuroscience 2002, *5 Suppl*, 1039–42.
32. Kashiwagi, K.; Masuko, T.; Nguyen, C. D.; Kuno, T.; Tanaka, I.; Igarashi, K.; Williams, K., Channel blockers acting at N-methyl-D-aspartate receptors: differential effects of mutations in the vestibule and ion channel pore. Molecular pharmacology 2002, *61* (3), 533–45.
33. Karakas, E.; Simorowski, N.; Furukawa, H., Subunit arrangement and phenylethanolamine binding in GluN1/GluN2B NMDA receptors. Nature 2011, *475* (7355), 249–253.
34. Ibrahim, L.; Diaz Granados, N.; Jolkovsky, L.; Brutsche, N.; Luckenbaugh, D. A.; Herring, W. J.; Potter, W. Z.; Zarate, C. A., Jr., A Randomized, placebo-controlled, crossover pilot trial of the oral selective NR2B antagonist MK-0657 in patients with treatment-resistant major depressive disorder. Journal of clinical psychopharmacology 2012, *32* (4), 551–7.
35. Pimlott, S. L.; Sutherland, A., Molecular tracers for the PET and SPECT imaging of disease. Chem Soc Rev 2011, *40* (1), 149–62.
36. Ametamey, S. M.; Honer, M.; Schubiger, P. A., Molecular imaging with PET. Chemical reviews 2008, *108* (5), 1501–16.
37. Fu, H.; Chen, Z.; Josephson, L.; Li, Z.; Liang, S. H., Positron Emission Tomography (PET) Ligand Development for Ionotropic Glutamate Receptors: Challenges and Opportunities for Radiotracer Targeting N-Methyl-d-aspartate (NMDA), α-Amino-3-hydroxy-5-methyl-4-isoxazolepropionic Acid (AMPA), and Kainate Receptors. Journal of medicinal chemistry 2019, *62* (2), 403–419.
38. Fuchigami, T.; Fujimoto, N.; Haradahira, T.; Nojiri, Y.; Okauchi, T.; Maeda, J.; Suhara, T.; Yamamoto, F.; Nakayama, M.; Maeda, M.; Mukai, T., Synthesis and characterization of (11) C-labeled benzyl amidine derivatives as PET radioligands for GluN2B subunit of the NMDA receptors. Journal of labelled compounds & radiopharmaceuticals 2018, *61* (14), 1095–1105.
39. Haider, A.; Herde, A. M.; Kramer, S. D.; Varisco, J.; Keller, C.; Frauenknecht, K.; Auberson, Y. P.; Temme, L.; Robaa, D.; Sippl, W.; Schibli, R.; Wunsch, B.; Mu, L.; Ametamey, S. M., Preclinical Evaluation of Benzazepine-Based PET Radioligands (R)- and (S)-(11)C-Me-NB1 Reveals Distinct Enantiomeric Binding Patterns and a Tightrope Walk Between GluN2B- and sigma(1)-Receptor-Targeted PET Imaging. Journal of nuclear medicine: official publication, Society of Nuclear Medicine 2019, *60* (8), 1167–1173.
40. Tewes, B.; Frehland, B.; Schepmann, D.; Schmidtke, K. U.; Winckler, T.; Wunsch, B., Design, Synthesis, and Biological Evaluation of 3-Benzazepin-1-ols as NR2B-Selective NMDA Receptor Antagonists. ChemMedChem 2010, *5* (5), 687–95.
41. Rischka, L.; Vraka, C.; Pichler, V.; Rasul, S.; Nics, L.; Gryglewski, G.; Handschuh, P.; Murgas, M.; Godbersen, G. M.; Silberbauer, L. R.; Unterholzner, J.; Wotawa, C.; Haider, A.; Ahmed, H.; Schibli, R.; Mindt, T.; Mitterhauser, M.; Wadsak, W.; Hahn, A.; Lanzenberger, R.; Hacker, M.; Ametamey, S. M., First-

in-Humans Brain PET Imaging of the GluN2B-Containing N-methyl-d-aspartate Receptor with (R)-(11)C-Me-NB1. Journal of nuclear medicine: official publication, Society of Nuclear Medicine 2022, *63* (6), 936–941.

42. Haider, A.; Iten, I.; Ahmed, H.; Muller Herder, A.; Gruber, S.; Kramer, S. D.; Keller, C.; Schibli, R.; Wunsch, B.; Mu, L.; Ametamey, S. M., Identification and Preclinical Evaluation of a Radiofluorinated Benzazepine Derivative for Imaging the GluN2B Subunit of the Ionotropic NMDA Receptor. Journal of nuclear medicine: official publication, Society of Nuclear Medicine 2018, *60* (2), 259–66.
43. Ahmed, H.; Haider, A.; Varisco, J.; Stankovic, M.; Wallimann, R.; Gruber, S.; Iten, I.; Hane, S.; Muller Herde, A.; Keller, C.; Schibli, R.; Schepmann, D.; Mu, L.; Wunsch, B.; Ametamey, S. M., Structure-Affinity Relationships of 2,3,4,5-Tetrahydro-1H-3-benzazepine and 6,7,8,9-Tetrahydro-5H-benzo[7]annulen-7-amine Analogues and the Discovery of a Radiofluorinated 2,3,4,5-Tetrahydro-1H-3-benzazepine Congener for Imaging GluN2B Subunit-Containing N-Methyl-d-aspartate Receptors. Journal of medicinal chemistry 2019, *62* (21), 9450–9470.
44. Ahmed, H.; Wallimann, R.; Haider, A.; Hosseini, V.; Gruber, S.; Robledo, M.; Nguyen, T. A. N.; Herde, A. M.; Iten, I.; Keller, C.; Vogel, V.; Schibli, R.; Wunsch, B.; Mu, L.; Ametamey, S. M., Preclinical Development of (18)F-OF-NB1 for Imaging GluN2B-Containing N-Methyl-d-Aspartate Receptors and Its Utility as a Biomarker for Amyotrophic Lateral Sclerosis. Journal of nuclear medicine: official publication, Society of Nuclear Medicine 2021, *62* (2), 259–265.
45. Smart, K.; Zheng, M. Q.; Ahmed, H.; Fang, H.; Xu, Y.; Cai, L.; Holden, D.; Kapinos, M.; Haider, A.; Felchner, Z.; Ropchan, J. R.; Tamagnan, G.; Innis, R. B.; Pike, V. W.; Ametamey, S. M.; Huang, Y.; Carson, R. E., Comparison of three novel radiotracers for GluN2B-containing NMDA receptors in non-human primates: (R)-[(11)C]NR2B-Me, (R)-[(18)F]of-Me-NB1, and (S)-[(18)F]of-NB1. J Cereb Blood Flow Metab 2022, *42* (8), 1398–1409.
46. Zheng, M.; Ahmed, H.; Smart, K.; Xu, Y.; Holden, D.; Kapinos, M.; Felchner, Z.; Haider, A.; Tamagnan, G.; Carson, R. E.; Huang, Y.; Ametamey, S. M., Characterization in nonhuman primates of (R)-[(18)F]OF-Me-NB1 and (S)-[(18)F]OF-Me-NB1 for imaging the GluN2B subunits of the NMDA receptor. Eur J Nucl Med Mol Imaging 2022, *49* (7), 2153–2162.
47. Ahmed, H.; Gisler, L.; Elghazawy, N. H.; Keller, C.; Sippl, W.; Liang, S. H.; Haider, A.; Ametamey, S. M., Development and Validation of [(3)H]OF-NB1 for Preclinical Assessment of GluN1/2B Candidate Drugs. Pharmaceuticals (Basel) 2022, *15* (8).
48. Szermerski, M.; Börgel, F.; Schepmann, D.; Haider, A.; Betzel, T.; Ametamey, S. M.; Wünsch, B., Fluorinated GluN2B Receptor Antagonists with a 3-Benzazepine Scaffold Designed for PET Studies. *ChemMedChem* 2018, *13* (10), 1058–1068.
49. Ahmed, H.; Zheng, M. Q.; Smart, K.; Fang, H.; Zhang, L.; Emery, P. R.; Gao, H.; Ropchan, J.; Haider, A.; Tamagnan, G.; Carson, R. E.; Ametamey, S. M.; Huang, Y., Evaluation of (rac)-, (R)-, and (S)-(18)F-OF-NB1 for Imaging GluN2B Subunit-Containing N-Methyl-d-Aspartate Receptors in Nonhuman Primates. Journal of nuclear medicine: official publication, Society of Nuclear Medicine 2022, *63* (12), 1912–1918.

50. Halder, R.; Ritter, T., (18)F-Fluorination: Challenge and Opportunity for Organic Chemists. J Org Chem 2021, *86* (20), 13873–13884.
51. Krishnan, H. S.; Ma, L.; Vasdev, N.; Liang, S. H., (18) F-Labeling of Sensitive Biomolecules for Positron Emission Tomography. *Chemistry* 2017, *23* (62), 15553–15577.
52. Deng, X.; Rong, J.; Wang, L.; Vasdev, N.; Zhang, L.; Josephson, L.; Liang, S. H., Chemistry for Positron Emission Tomography: Recent Advances in (11) C-, (18) F-, (13) N-, and (15) O-Labeling Reactions. Angew Chem Int Ed Engl 2019, *58* (9), 2580–2605.
53. van der Born, D.; Pees, A.; Poot, A. J.; Orru, R. V. A.; Windhorst, A. D.; Vugts, D. J., Fluorine-18 labelled building blocks for PET tracer synthesis. Chem Soc Rev 2017, *46* (15), 4709–4773.
54. Zischler, J.; Kolks, N.; Modemann, D.; Neumaier, B.; Zlatopolskiy, B. D., Alcohol-Enhanced Cu-Mediated Radiofluorination. Chemistry 2017, *23* (14), 3251–3256.
55. Ishiyama, T.; Murata, M.; Miyaura, N., Palladium(0)-Catalyzed Cross-Coupling Reaction of Alkoxydiboron with Haloarenes: A Direct Procedure for Arylboronic Esters. The Journal of Organic Chemistry 1995, *60* (23), 7508–7510.
56. Merritt, E. A.; Olofsson, B., Diaryliodonium salts: a journey from obscurity to fame. Angew Chem Int Ed Engl 2009, *48* (48), 9052–70.
57. Rotstein, B. H.; Stephenson, N. A.; Vasdev, N.; Liang, S. H., Spirocyclic hypervalent iodine(III)-mediated radiofluorination of non-activated and hindered aromatics. Nat Commun 2014, *5*, 4365.
58. Shah, A.; W. Pike, V.; A. Widdowson, D., The synthesis of [18F]fluoroarenes from the reaction of cyclotron-produced [18F]fluoride ion with diaryliodonium salts. Journal of the Chemical Society, Perkin Transactions *1* 1998, (13), 2043–2046.
59. Heck, R. F.; Nolley, J. P., Jr., Palladium-catalyzed vinylic hydrogen substitution reactions with aryl, benzyl, and styryl halides. The Journal of Organic Chemistry 1972, *37* (14), 2320–2322.
60. van Gemmeren, M.; Börjesson, M.; Tortajada, A.; Sun, S. Z.; Okura, K.; Martin, R., Switchable Site-Selective Catalytic Carboxylation of Allylic Alcohols with CO(2). Angew Chem Int Ed Engl 2017, *56* (23), 6558–6562.
61. Lauer, M. G.; Thompson, M. K.; Shaughnessy, K. H., Controlling olefin isomerization in the heck reaction with neopentyl phosphine ligands. J Org Chem 2014, *79* (22), 10837–48.
62. Roelofsen, D. P.; Wils, E. R. J.; van Bekkum, H., Synthesis of acetals using molecular sieves. Recueil des Travaux Chimiques des Pays-Bas 1971, *90* (10), 1141–1152.
63. Takahashi, I.; Hayashi, M.; Fujita, T.; Ichikawa, J., Brønsted Acid-catalyzed Tandem Cycloaromatization of Naphthalene-based Bisacetals: Selective Synthesis of ortho-Fused Six-hexagon Benzenoids. Chemistry Letters 2017, *46* (3), 392–394.
64. Sun, J.; Dong, Y.; Cao, L.; Wang, X.; Wang, S.; Hu, Y., Highly efficient chemoselective deprotection of O,O-acetals and O,O-ketals catalyzed by molecular iodine in acetone. J Org Chem 2004, *69* (25), 8932–4.

65. Paoletti, P.; Bellone, C.; Zhou, Q., NMDA receptor subunit diversity: impact on receptor properties, synaptic plasticity and disease. Nature Reviews Neuroscience 2013, *14* (6), 383–400.
66. Niso, M.; Pati, M. L.; Berardi, F.; Abate, C., Rigid versus flexible anilines or anilides confirm the bicyclic ring as the hydrophobic portion for optimal σ2 receptor binding and provide novel tools for the development of future σ2 receptor PET radiotracers. RSC Advances 2016, *6* (91), 88508–88518.
67. Logan, J.; Fowler, J. S.; Volkow, N. D.; Wang, G. J.; Ding, Y. S.; Alexoff, D. L., Distribution volume ratios without blood sampling from graphical analysis of PET data. J Cereb Blood Flow Metab 1996, *16* (5), 834–40.
68. Kramer, S. D.; Betzel, T.; Mu, L.; Haider, A.; Herde, A. M.; Boninsegni, A. K.; Keller, C.; Szermerski, M.; Schibli, R.; Wunsch, B.; Ametamey, S. M., Evaluation of (11)C-Me-NB1 as a Potential PET Radioligand for Measuring GluN2B-Containing NMDA Receptors, Drug Occupancy, and Receptor Cross Talk. Journal of nuclear medicine: official publication, Society of Nuclear Medicine 2018, *59* (4), 698–703.
69. *Science Translational Medicine* **2022**, *14* (630), eabm3682.
70. Bertoglio, D.; Verhaeghe, J.; Korat, Š.; Miranda, A.; Wyffels, L.; Stroobants, S.; Mrzljak, L.; Dominguez, C.; Liu, L.; Skinbjerg, M.; Munoz-Sanjuan, I.; Staelens, S., In vitro and In vivo Assessment of Suitable Reference Region and Kinetic Modelling for the mGluR1 Radioligand [(11)C]ITDM in Mice. Mol Imaging Biol 2020, *22* (4), 854–863.

## Schemes

Schemes 1-3 are available in the supplementary files section.

## Supplementary Information

Supporting Information not available with this version.

## Figures

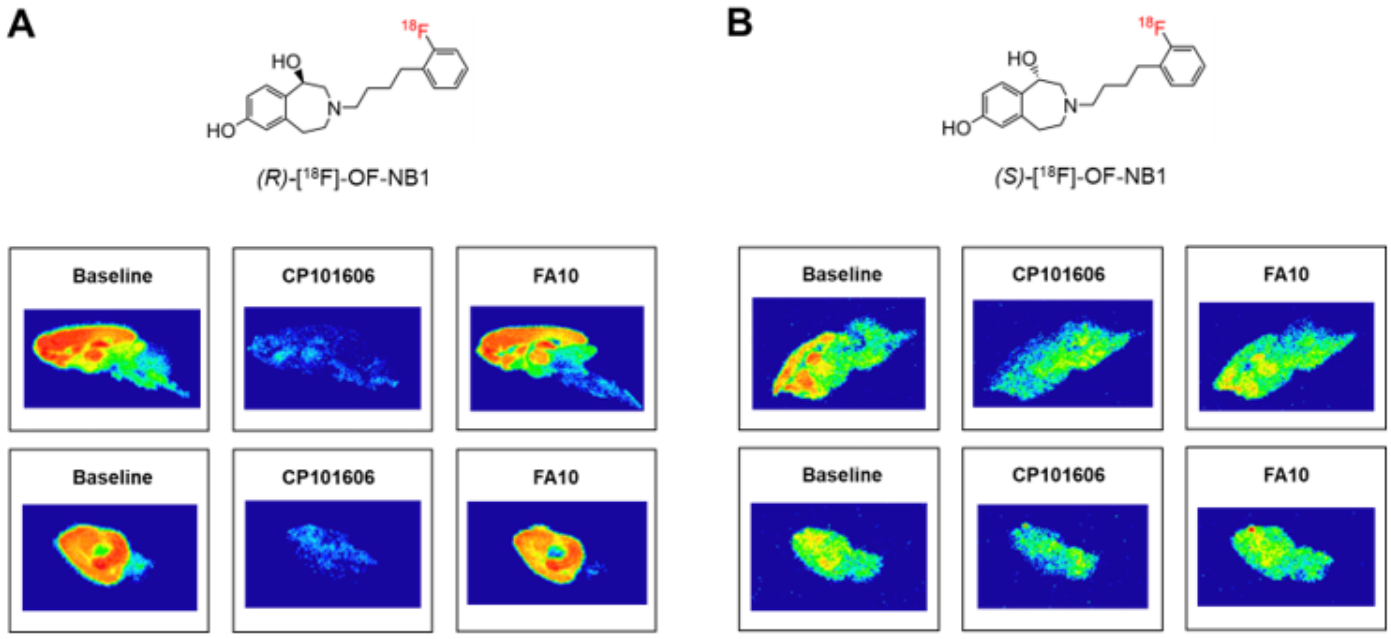


## Figure 1

Representative in vitro autoradiography of rat (upper panel) and mouse (lower panel) brains. **A.** Autoradiograms after incubation with (R)-[$^{18}$F]OF-NB1 only (baseline) or in combination with GluN2B antagonist, CP101,606 (10 μM). Selectivity over sigma2 receptors was assessed by blockade studies with FA10 (10 μM). **B.** Autoradiograms after incubation with (S)-[$^{18}$F]OF-NB1 alone or in combination with GluN2B antagonist, CP101,606 (10 μM). FA10 (10 μM) was used to assess selectivity over sigma2 receptors.

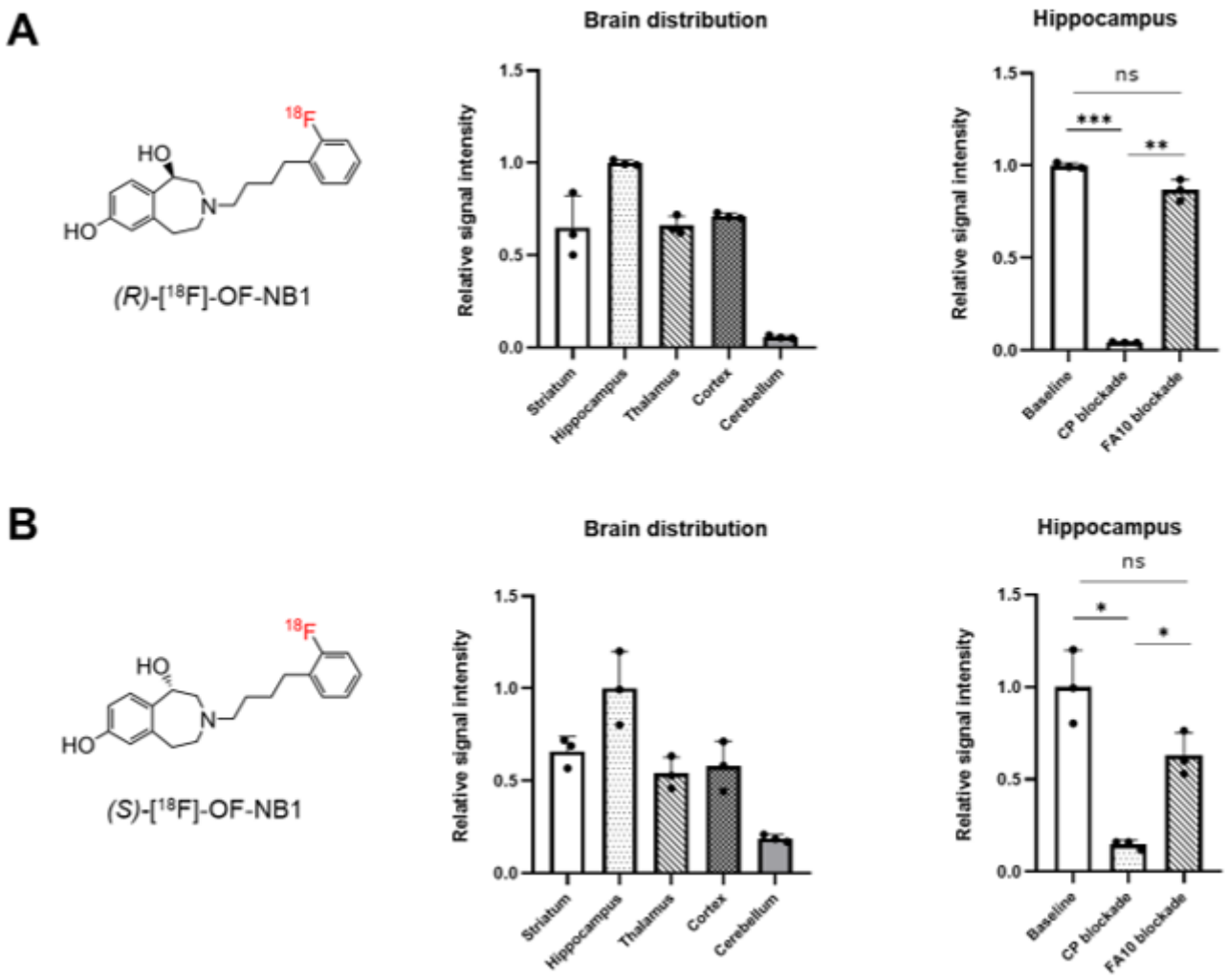


## Figure 2

Quantification of autoradiographic data from rat brain sections. **A**. Distribution of (R)-[$^{18}$F]OF-NB1 throughout distinct brain regions. GluN2B subunit-specificity was derived from the extent of signal reduction from baseline to CP (CP101,606) blockade. Selectivity over sigma2 receptors was assessed by the extent of signal reduction from baseline to FA10 blockade. **B**. Distribution of (S)-[$^{18}$F]OF-NB1 throughout distinct brain regions. GluN2B subunit-specificity was derived from the extent of signal reduction from baseline to CP (CP101,606) blockade. Selectivity over sigma2 receptors was assessed by the extent of signal reduction from baseline to FA10 blockade.

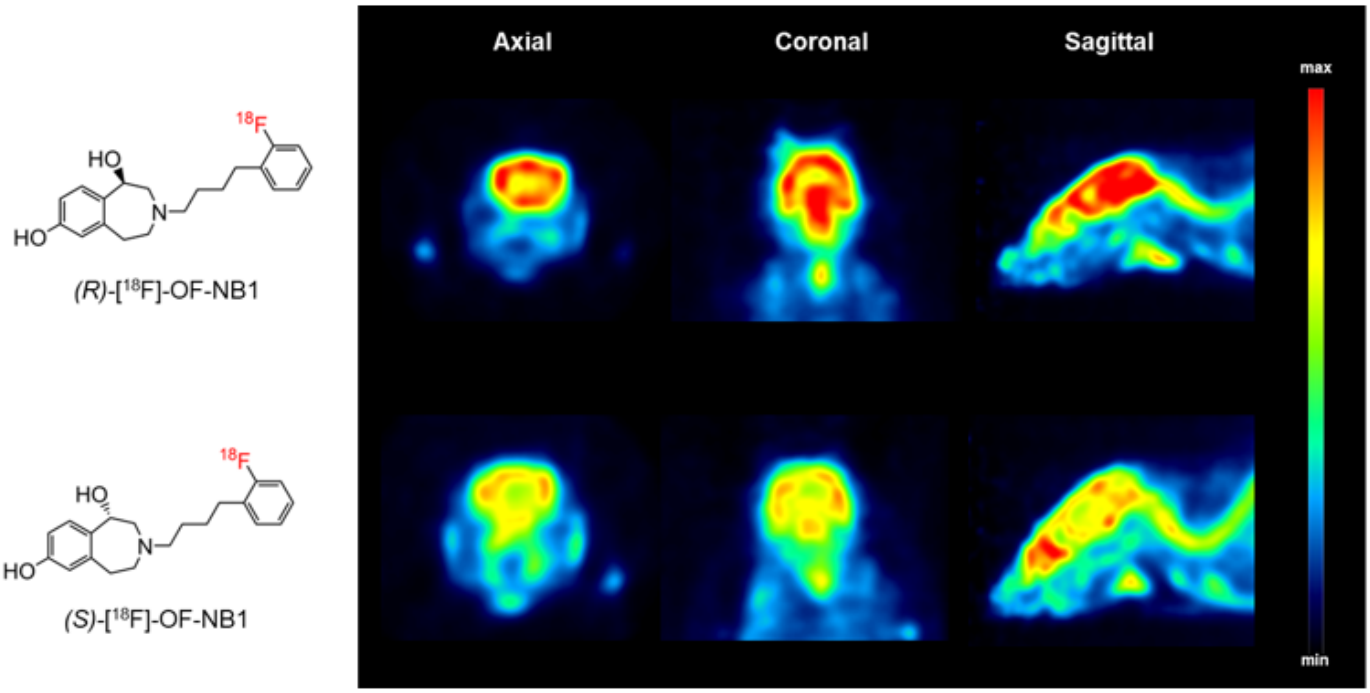


## Figure 3

Representative positron emission tomography (PET) images of the mouse brain from an axial, coronal and sagittal view. **A.** Mouse brain images following tail-vein injection of (R)-[$^{18}$F]OF-NB1. **B.** Mouse brain images following tail-vein injection of (S)-[$^{18}$F]OF-NB1.

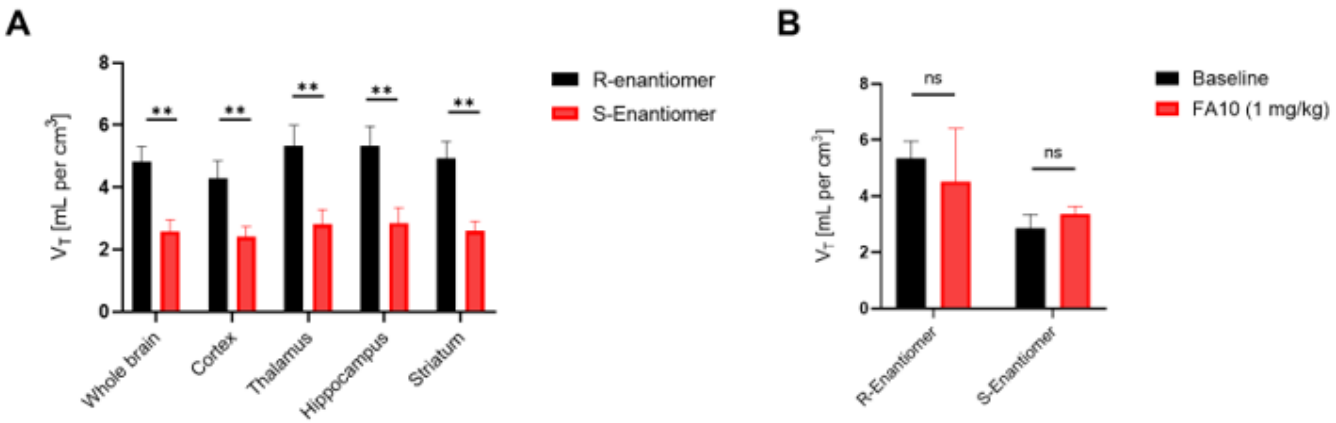


## Figure 4

Quantification of (R)-[$^{18}$F]OF-NB1 and (S)-[$^{18}$F]OF-NB1 volumes of distribution ($V_T$) across different mouse brain regions, calculated via Logan graphical analysis. **A**. Comparison of (R)-[$^{18}$F]OF-NB1 vs. (S)-[$^{18}$F]OF-NB1 retention in the whole brain, as well as in GluN2B subunit-expressing regions. **B.**

Hippocampal volumes of distribution for (R)-[$^{18}$F]OF-NB1 and (S)-[$^{18}$F]OF-NB1 at baseline and following challenge with sigma2 receptor ligand, FA10 (1 mg/kg).

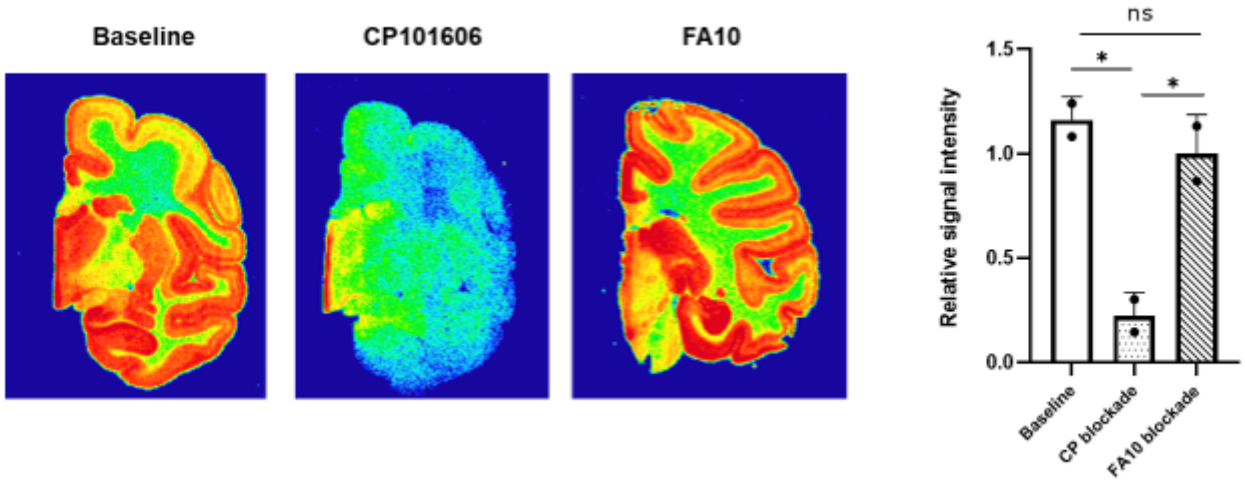


**Figure 5**

Representative in vitro autoradiograms of (R)-[$^{18}$F]OF-NB1 on post-mortem non-human primate (NHP) brain tissue sections. For specificity testing, GluN2B antagonist, CP101,606, was used in a concentration of 10 μM. Selectivity over sigma2 receptors was assessed using FA10 (10 μM).

# Supplementary Files

This is a list of supplementary files associated with this preprint. Click to download.

- Schemes.docx